Editors' Suggestion | Featured in Physics

Model of Active Solids: Rigid Body Motion and Shape-Changing Mechanisms

Claudio Hernández-López,[1,4,*] Paul Baconnier,[2] Corentin Coulais,[3] Olivier Dauchot,[2] and Gustavo Düring[4,†]
[1]Laboratoire de Physique de l'École Normale Supérieure, UMR CNRS 8023, Université PSL, Sorbonne Université, 75005 Paris, France
[2]Gulliver UMR CNRS 7083, ESPCI Paris, Université PSL, Paris, France
[3]Institute of Physics, Universiteit van Amsterdam, 1098 XH Amsterdam, The Netherlands
[4]Instituto de Física, Pontificia Universidad Católica de Chile, 8331150 Santiago, Chile

(Received 21 October 2023; revised 26 January 2024; accepted 3 April 2024; published 7 June 2024)

Active solids such as cell collectives, colloidal clusters, and active metamaterials exhibit diverse collective phenomena, ranging from rigid body motion to shape-changing mechanisms. The nonlinear dynamics of such active materials remains, however, poorly understood when they host zero-energy deformation modes and when noise is present. Here, we show that stress propagation in a model of active solids induces the spontaneous actuation of multiple soft floppy modes, even without exciting vibrational modes. By introducing an adiabatic approximation, we map the dynamics onto an effective Landau free energy, predicting mode selection and the onset of collective dynamics. These results open new ways to study and design living and robotic materials with multiple modes of locomotion and shape change.

DOI: 10.1103/PhysRevLett.132.238303

Polar active matter is composed of self-driven units that convert energy into directed motion or forces. Aligning interactions among the active units lead to large-scale collective motion in various forms, from polar flocks of birds [1,2], motile colloids [3], vibrated disks [4], interacting robots [5–7], and vortex flows of fish [8], bacteria [9], or colloids [10,11], to quote only a few. The large-scale physics of these flows has been the topic of intensive research and is well described by the so-called Toner-Tu equations [12,13]. When the density of active units is large because of confinement [14] or cohesion [15,16], the structure of the assembly may remain frozen on long timescales, and the system exhibits elastic rather than viscous properties. When cohesive interactions are large enough, as is the case for dense biofilms [17], keratocyte swarms [18], or epithelial monolayers [19], active units can be considered embedded in an elastic network, in a way similar to artificially designed active elastic metamaterials [20–23].

A natural starting point is then to analyze the dynamics in terms of the vibrational modes of the elastic medium or structure, with the zero modes corresponding to node displacements that do not change any bond length [24]. It was shown that correlated noise generated by an active matter bath can actuate a nontrivial zero mode while suppressing harmonic modes to a degree dependent on temporal correlations [21]. Self-propulsion is further able to mobilize solid body motion [20] or a free-moving mechanism even in a topologically complex case [21]. Notably, observations on *Placozoa phylum* [25], a living active solid, have revealed global rotation and translations under various conditions. Finally, in the presence of a nonlinear feedback of the elastic stress on the orientation of the active forces, self-propulsion can also actuate a few selected harmonic modes [22]. Yet the selection mechanism remains unclear. More generally, in the presence of several actuatable modes, whether trivially associated with solid body motion or more complex mechanisms, several dynamics coexist in phase space, and there is to date no general principle to characterize their metastability.

In this Letter, we provide a general formalism to describe the statistical evolution of collective motion, in the case where several zero modes are present, as illustrated in Fig. 1, using the hexbug elastic network [Fig. 1(a)], introduced in [22]. When the network is pinned in the center and the translational solid body motion is forbidden, the only remaining zero mode is rotation [Fig. 1(b)]. The dynamics breaks chiral symmetry by spontaneously selecting one direction of rotation, which eventually reverses in the presence of noise. When the network is not pinned, there are two translational and one rotational zero modes, which also spontaneously break the continuous rotational, *XY* model-like, and chiral, Ising-like, symmetries. Both translational [Fig. 1(c)] and rotational motion [Fig. 1(d)] are observed depending on the initial conditions. Transitions between the two types of motion are observed numerically [Fig. 1(e)]. The excitations associated with these broken continuous symmetries are analogous to Goldstone modes in condensed matter theories. Finally, Fig. 1(f) shows the dynamics of a nontrivial active mechanism with two zero modes: an ideal auxetic network [26–29] pinned at the center that can freely rotate and contract.

When the timescales of the dynamics are much longer than the elastic relaxation time, as is the case here, the

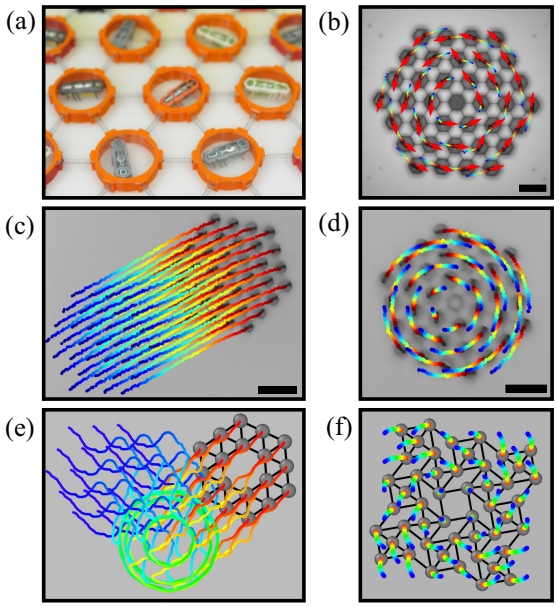

FIG. 1. Active rigid body motion and active mechanisms. (a) Enlargement of the experimental active elastic lattice introduced in [22], with self-propelling units—hexbugs—trapped in 3D-printed annuli, connected by springs in a triangular lattice. (b) Experimental rotational dynamics observed under central pinning. Scale bar, 10 cm. (c),(d) Experimental translational and rotational dynamics observed for a free structure. Scale bar, 20 cm. (e) Alternating translational and rotation dynamics obtained numerically for the same free structure. (f) A rotational-auxetic regime observed numerically for a nonpinned auxetic square system (see the text, Fig. 3, and Movie S1 [30]). Trajectories are color coded from blue to red by increasing time.

harmonic modes of the solid are barely excited and the network can be considered as rigid. We show first that in this limit stress propagation is enough to induce collective motion: At small enough noise, the symmetric phase is spontaneously broken, and the evolution of the system follows a specific path along the zero mode space. This introduces a new timescale, which competes with the timescale of reorientation of the active particles. We prove that, within an adiabatic approximation, the dynamics is governed by an effective Landau free energy, from which the mode selection and the metastability can be easily understood. Our results pave the way toward active metamaterials with multiple modes of actuation and locomotion [31].

We consider active systems described by the overdamped dynamics of N self-aligning units, which were introduced independently in several contexts [4,14,15,18,22,32]. Written in nondimensional units (see Supplemental Material [30], Sec. I, for details), the equations read

$$\dot{\boldsymbol{x}}_i = \hat{\boldsymbol{n}}_i + \boldsymbol{F}_i, \tag{1}$$

$$\dot{\theta}_i = \frac{1}{\pi_r}(\hat{\boldsymbol{n}}_i^{\perp} \cdot \boldsymbol{F}_i) + \sqrt{2\pi_\theta/\pi_r}\,\xi_i, \tag{2}$$

with $\boldsymbol{x}_i$, respectively, $\hat{\boldsymbol{n}}_i = (\cos\theta_i, \sin\theta_i)$, the position and the polarization unit vector of active unit i. $\boldsymbol{F}_i$ is the net external force on unit i. The dimensionless self-alignment length $\pi_r = \ell_a/\ell_0$ is the ratio between the self-alignment length ℓ_a and the characteristic agent-agent distance ℓ_0. The dimensionless noise coefficient corresponds to $\pi_\theta = D_\theta \ell_a / v_0$, with v_0 the speed of a free agent and D_θ the angular diffusion coefficient. We define ξ_i as a delta-correlated Gaussian white noise process. The self-aligning torque, on the right-hand side of Eq. (2), emerges from nonsymmetric dissipative forces with respect to $\hat{\boldsymbol{n}}_i$, when it is misaligned with $\dot{\boldsymbol{x}}_i$ [32]. It was shown to be the key ingredient for the onset of collective motion in active disks [4] and collective actuation in active elastic networks [22].

One can show (see Supplemental Material [30], Sec. I) that the network can be safely considered rigid provided

$$\frac{\ell_e}{\ell_a} \ll \frac{1}{k}\omega_q^2, \quad \forall\ q \in \{1\ldots, 2N\} \tag{3}$$

where ℓ_e is the amplitude of the typical displacement of the nodes resulting from the active forces and ω_q^2 are the nonzero eigenvalues of the dynamical matrix [24]. As such, the bound for activation of the elastic modes depends on only the geometry of the structure. In the following, we shall perform all simulations with parameters such that the rigid approximation holds.

We start by simulating three systems with a single zero mode (Fig. 2): (i) a crystalline triangular lattice with periodic boundary conditions (PBCs), (ii) a triangular lattice pinned at its center, and (iii) an ideal auxetic network pinned at its center, illustrated in Figs. 2(a), 2(e), and 2(i), respectively. All of them exhibit collective motion along their single zero mode at small noise. The triangular lattice with PBCs translates uniformly, with a nonzero magnitude of the global polarization $\boldsymbol{P} = (1/N)\sum_i \hat{\boldsymbol{n}}_i$ [Fig. 2(b)]. The network pinned at the center freely rotates, with an angular speed $\dot{\phi}$, that randomly switches from counterclockwise to clockwise rotation [Fig. 2(f)]. The auxetic network freely compresses with a finite auxetic angular speed $\dot{\gamma}$ [Fig. 2(j)]. In all cases, collective motion emerges from a spontaneous symmetry breaking of the disordered phase, when $\pi_\theta < 1/2$ [Figs. 2(c), 2(g), and 2(k)].

The situation becomes more interesting when the network of interest has more than one zero mode; see Fig. 3. An active network free of PBCs has both translational and rotational zero modes. The simulations reveal that, at low π_θ, the collective dynamics switches between pure translations and pure rotation [Fig. 3(a)]. As the rotational state is characterized by a vortexlike defect in the polarity field, these transitions amount to the spontaneous formation or annihilation of defects under the influence of noise. Boundary conditions are determinant, allowing changes in the net topological charge (free), fixing defect localization (pinned), or forbidding their creation (periodic). The case of an auxetic network that is also free to rotate is even more

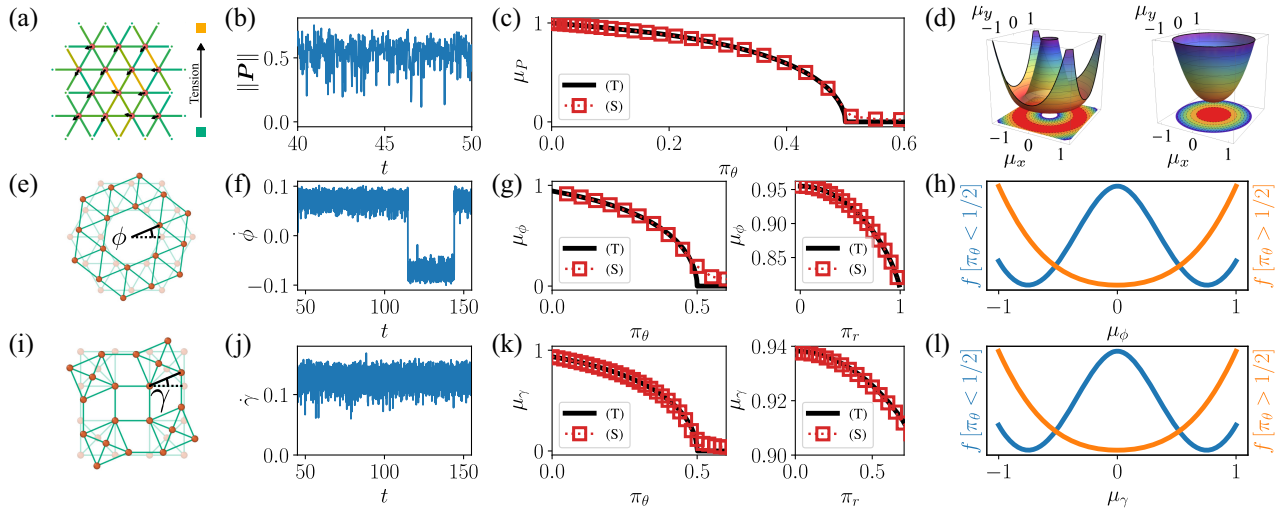

FIG. 2. Second-order transitions to solid body motion and mechanisms for one-mode systems. Simulations consider $\pi_r = 0.001$ unless specified. (a) Periodic boundary condition (translation-only) network. (b)–(d) consider a 100×100 translating system. (b) Global polarization magnitude $\|\boldsymbol{P}\|$ time series; $\pi_\theta = 0.4$. (c) Phase diagram μ_P vs π_θ as a function of noise. (S) for simulations, (T) for theoretical predictions. (d) Landau free energy as a function of μ_x and μ_y; left: $\pi_\theta = 0.1$; right: $\pi_\theta = 0.6$. (e) A two-layer hexagonal ring with the definition of the rotational angle ϕ. (f)–(h) consider a nine-layer hexagonal ring system. (f) Angular velocity $\dot{\phi}$ time series; $\pi_\theta = 0.4$. (g) Phase diagram μ_ϕ vs π_θ (left) and μ_ϕ vs π_r, when $\pi_\theta = 0$ (right). (h) Landau free energy as a function of μ_ϕ; blue: $\pi_\theta = 0.25$; orange: $\pi_\theta = 0.6$. (i) A one-layer auxetic system with the definition of the auxetic angle γ. (j)–(l) consider an eight-layer auxetic system. (j) Auxetic angular velocity $\dot{\gamma}$ time series; $\pi_\theta = 0.4$. (k) Phase diagram μ_γ vs π_θ (left) and μ_γ vs π_r, when $\pi_\theta = 0$ (right). (l) Landau free energy as a function of μ_γ. Blue: $\pi_\theta = 0.25$; orange: $\pi_\theta = 0.6$.

complex. As we shall see, this is because the rotational mode depends on the distance of the particles to the center, which changes while the system evolves along the auxetic mode. The visual inspection of the auxetic and rotation rates as a function of time for different values of π_θ indicates that in the limit of vanishing noise, $\dot{\phi}$ remains constant, and $\dot{\gamma}$ fluctuates periodically. Increasing the noise, transitions between two states with different $\dot{\phi}$ signs can be achieved, and even larger noise values lead to a state where such transitions occur constantly [Fig. 3(d)].

We now come to the theoretical analysis of the above observations. For a rigid network, the bond elongations are null. Imposing such distance-preserving condition to Eq. (1), one finds after some algebra (see Supplemental Material [30], Sec. II)

$$\boldsymbol{F}_i = -\hat{\boldsymbol{n}}_i + \sum_{q \in \mathfrak{F}} \langle \boldsymbol{\varphi}^q | \hat{\boldsymbol{n}} \rangle \boldsymbol{\varphi}_i^q, \tag{4}$$

where $\boldsymbol{\varphi}_i^q$ is the vector associated with particle i in the qth eigenmode of the dynamical matrix of the elastic network and $\mathfrak{F}$ is the set of zero modes. Note that self-stress states, i.e., stress configurations in the null space of the equilibrium matrix [24], do not contribute to this net force and, thus, do not influence the behavior of the system. Then, replacing the force in Eqs. (1) and (2),

$$\dot{\boldsymbol{x}}_i = \sum_{q \in \mathfrak{F}} \langle \boldsymbol{\varphi}^q | \hat{\boldsymbol{n}} \rangle \boldsymbol{\varphi}_i^q \quad \text{and} \quad \dot{\theta}_i = -\frac{1}{\pi_r} \frac{\partial V}{\partial \theta_i} + \sqrt{\frac{2\pi_\theta}{\pi_r}} \xi_i, \tag{5}$$

with $V = -\frac{1}{2} \sum_{q \in \mathfrak{F}} \langle \boldsymbol{\varphi}^q | \hat{\boldsymbol{n}} \rangle^2$. The stochastic dynamics is then described by the time-dependent probability density $Q(\boldsymbol{x}_1, \ldots, \boldsymbol{x}_N; \theta_1, \ldots, \theta_N; t)$, which evolves according to the Fokker-Planck equation:

$$\frac{\partial Q}{\partial t} = \frac{1}{\pi_r} \frac{\partial}{\partial \theta_i} \left(\frac{\partial V}{\partial \theta_i} Q + \pi_\theta \frac{\partial Q}{\partial \theta_i} \right) - \boldsymbol{\nabla}_{\boldsymbol{x}_i} (\langle \boldsymbol{\varphi}^q | \hat{\boldsymbol{n}} \rangle \boldsymbol{\varphi}_i^q Q) \tag{6}$$

with implicit summation on the indices. The evolution of the M zero modes can be described with a set of angles, distances, or more general coordinates, which we denote $\boldsymbol{\alpha} = \{\alpha_m\}_{m=1}^M$. To make further progress, we proceed to an adiabatic approximation, assuming that the dynamics of the zero modes is much slower than that of the orientation of the active units, which is expected to hold in the $\pi_r \ll 1$ regime. At zeroth order, this approximation amounts to considering that the probability density function Q is different from zero only for combinations of $\boldsymbol{x}_i$ which preserve the same zero modes. In such a case, the Fokker-Planck equation for the reduced density probability function $\mathcal{Q} = \int_{-\infty}^{\infty} Q d\boldsymbol{x}_1 \ldots d\boldsymbol{x}_N$ admits a steady state solution given by the Gibbs measure:

$$\mathcal{Q} = \frac{\exp(-\beta V)}{\mathcal{Z}} \tag{7}$$

with $\beta = 1/\pi_\theta$ and $\mathcal{Z} = \int_{-\pi}^{\pi} e^{-\beta V} \mathrm{d}\theta_1 \ldots \mathrm{d}\theta_N$.

Collective motion is achieved when the normalized projections of the polarity vectors over the zero modes;

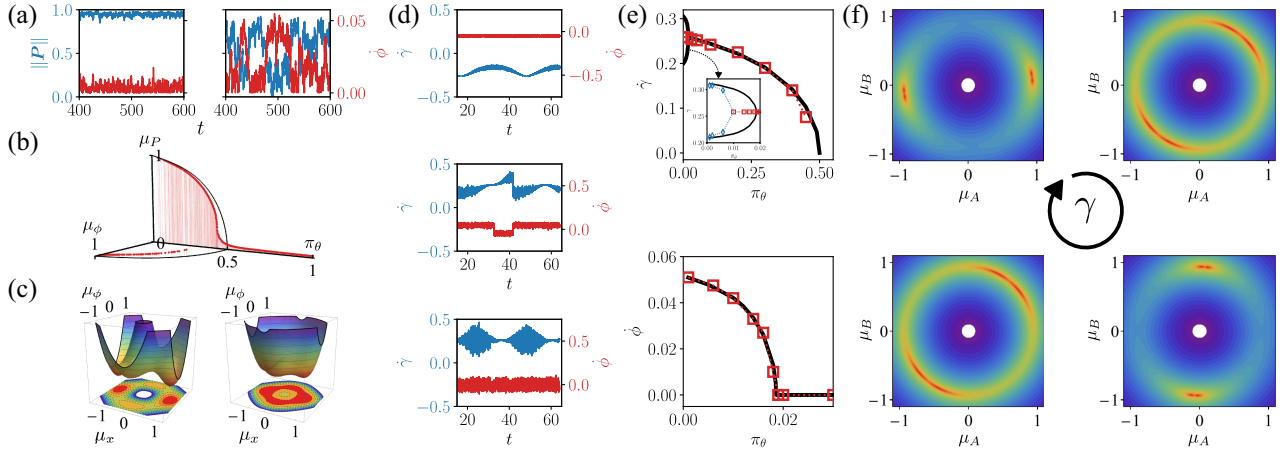

FIG. 3. Two-mode system phenomenology: switching between modes of actuation. (a) Time series of the magnitude of the global polarization $\boldsymbol{P}$ (blue) and of the angular velocity $\dot{\phi}$ (red) for a two-ring nonpinned triangular lattice; left to right: $\pi_\theta = 0.10$, 0.35; $\pi_r = 0.1$. (b) Phase diagram μ_P and μ_ϕ vs π_θ of a 30-ring nonpinned triangular lattice. (c) Landau free energy for a nonpinned two-ring triangular lattice as a function of μ_ϕ and μ_x; from left to right: $\pi_\theta = 0.10$, 0.35. (d)–(f) consider an eight-layer rotational-auxetic network. (d) Time series of the auxetic angular velocity $\dot{\gamma}$ (blue) and rotational angular velocity $\dot{\phi}$ (red); from top to bottom: $\pi_\theta = 0.001$, 0.006, 0.014. (e) Phase diagram $\dot{\gamma}$ (top) and $\dot{\phi}$ (bottom) vs π_θ. The theoretical values are the time average of each solution obtained from following the free energy minima as γ varies. Inset: enlargement of the $\dot{\phi} \neq 0$ region. (f) Landau free energy as it varies with γ ($\gamma = 0.2 + n\pi/2$, with $n = 0$, 1, 2, 3); $\pi_\theta = 0.001$, and the evolution time step $\Delta t = 0.01$.

namely, the order parameters $\mu_q = \langle(\sum_i \boldsymbol{\varphi}_i^q \cdot \hat{\boldsymbol{n}}_i)\rangle/\sqrt{N}$ are $\mathcal{O}(1)$. In the thermodynamic limit, and considering the case of extended zero modes, such as translations, rotations, or auxetic modes [28], we find that the mode selection is governed by the minimum of the Landau free energy:

$$f[\boldsymbol{\mu}, \boldsymbol{\alpha}] = \sum_{q \in \mathfrak{F}} \frac{\mu_q^2}{2} - \frac{1}{\beta N} \sum_i \log\left(I_0(\beta \mathcal{D}_i)\right), \tag{8}$$

where I_0 is the modified Bessel function of the first kind and

$$\mathcal{D}_i = \left(N \sum\nolimits_{q,l \in \mathfrak{F}} \mu_q \mu_l (\boldsymbol{\varphi}_i^q(\boldsymbol{\alpha}) \cdot \boldsymbol{\varphi}_i^l(\boldsymbol{\alpha}))\right)^{1/2} \tag{9}$$

couples the different zero modes. Finally, having found the order parameters for a particular system configuration $\boldsymbol{\alpha}$, we can evolve every α_m as $\dot{\alpha}_m = L_m(\boldsymbol{\alpha}, \boldsymbol{\mu})$, where L_m is a structure-dependent operator.

Using the above formulation, we can prove that, within the adiabatic approximation, for any system with extended zero modes, there is a continuous phase transition from a disordered phase to some form of collective motion, taking place at $\pi_\theta^c = 1/2$. This description, valid only in the large N limit, can be extended to small N in terms of simple integrals and higher-order corrections as powers of π_r can also be found (see Supplemental Material [30], Secs. IV and VI).

The simplest scenario corresponds to pure translational motion. If no other zero mode is allowed, as is the case for an unpinned lattice with PBCs, the zeroth-order solution [Eq. (7)] is exact, because the translational modes are position independent. The order parameter is $\boldsymbol{\mu}_P = (\mu_x, \mu_y) = \langle(1/N)\sum_i \hat{\boldsymbol{n}}_i\rangle$. The angular potential reads $V = -(1/2N)\sum_{i,j}\cos(\theta_i - \theta_j)$ and, therefore, exactly maps onto the 2D mean-field XY model. The minima of the corresponding free energy shown in Fig. 2(d) for two noise amplitudes perfectly captures the transition. In the thermodynamic limit, a phase transition at $\pi_\theta = 1/2$ with the mean-field critical exponents is obtained (see Supplemental Material [30], Sec. IV). Remarkably, the mean-field behavior does not arise from an uncontrolled approximation: True long-range order emerges from systemwide stress propagation, resulting from rigidity (see Movie S2 [30]).

In the purely rotational, or auxetic cases, the adiabatic approximation is not exact, because the associated zero modes depend on the instantaneous structure prescribed by ϕ, the rotational angle, and γ, the compression angle [see Figs. 2(e) and 2(i)]. However, in the presence of a single zero mode, an adequate choice of reference frame removes this dependence. Here also we find a perfect agreement between the simulation data [Figs. 2(g) and 2(k)] and the order parameters μ_ϕ and μ_γ extracted from the minimization of the free energy shown in Figs. 2(h) and 2(l) (see Supplemental Material [30], Secs. VI and VII). The dependence of these so-defined order parameters on π_r, when $\pi_\theta = 0$, is also perfectly captured [see Figs. 2(g) and 2(k) and Supplemental Material [30], Secs. VI and VII].

Two-mode settings lead to more intricate dynamics and complex energy landscapes. First, we will consider a translational-rotational system that has a Landau free energy that is independent of the structure parameter, an

exception due to the structure-invariant nature of the translational modes. The order parameters are the ones defined for the pure translation and rotational case. The free energy, however, displays a richer behavior, when $\pi_\theta < \pi_\theta^c = 1/2$: The space isotropy for translation and the chiral symmetry for rotation are simultaneously broken [see Fig. 3(b) and Movie S3 [30]]. Interestingly, the translational solution is always the global minimum [see Fig. 3(c) and Supplemental Material [30], Sec. VIII], and mixed translational and rotational states are not steady state solutions. The mean-field nature of the system leads to minima that are separated by an energy barrier proportional to N.

Finally, considering a network where the two zero modes are the rotation and the auxetic one allows us to demonstrate the efficiency of our approach while stressing its limitations. Our prescription eliminates the dependence on ϕ and defines the two order parameters μ_A and μ_B as functions of $\langle\dot{\phi}\rangle$, $\langle\dot{\gamma}\rangle$, and γ (see Supplemental Material [30], Sec. IX). Depending on the value of π_θ, the free energy has four local minima, two, or just one, i.e., the disordered solution. As shown in Fig. 3(f), these minima move in phase space as γ evolves. For a given set π_θ, π_r, we can follow the evolution of each different solution from the adiabatic prescription $\dot{\alpha}_m = L_m(\boldsymbol{\alpha}, \boldsymbol{\mu})$ (see Supplemental Material [30], Sec. IX). This adiabatic evolution converges to a well-defined phase diagram [see Fig. 3(e)] that remarkably displays two transitions, the aforementioned one at $\pi_\theta^c = 1/2$, where the auxetic contraction is activated, and a second one at much smaller values, $\pi_\theta \approx 0.02$, where rotation is activated. Numerical simulations of the auxetic-rotation systems show good agreement in most of the phase diagram, except in the region below the onset of rotational dynamics [see the inset in Fig. 3(e)], where the system evolves following two minima that are separated by a low, vanishing for large N, energy barrier. An appropriate numerical procedure to follow the evolution of the structure should solve this discrepancy.

In this Letter, we have studied the dynamics of active solid body motion and mechanism folding through a general theoretical framework in the rigid limit. Our formalism allows for the design and tuning of a wide range of materials where elastic deformations are negligible, with the interaction between different modes giving rise to rich, complex dynamics. Future work will restore elasticity, in particular, elucidating whether long-range order is preserved for different system sizes and spring constants. In opposition to the rigid case, where stresses can propagate infinitely far and instantaneously, overcoming the Mermin-Wagner theorem with elastic interactions is not trivial. Numerical studies on a related model seem to suggest that stiff enough systems display collective motion independently of the system size [25], and, in such a case, corrections beyond mean field could be calculated. Furthermore, we will explore structures with multiple shape-changing modes [33] and settings with various active solids or environmental obstacles and consider our dynamical system outside the $\pi_r \ll 1$ limit, potentially capturing other effects such as the geometry-controlled selection of particular translation directions [5]. This nonadiabatic regime, and a coarse-grained description of our order parameters to properly deal with inhomogeneities in our system beyond mean field, could be suited to further study the formation and dynamics of defects in the polarity field.

C. H.-L. was supported by a Ph.D. grant from ED564 "Physique en Ile de France." G. D. acknowledges support from Fondecyt Grant No. 1210656. P. B. was supported by a Ph.D. grant from ED564 "Physique en Ile de France." C. C. acknowledges funding from the European Research Council under Grant Agreement No. 852587 and from the Netherlands Organisation for Scientific Research under Grant Agreement No. VIDI 2131313.

*claudio.hernandez.lopez@bio.ens.psl.eu
†gduring@uc.cl

[1] A. Cavagna, A. Cimarelli, I. Giardina, G. Parisi, R. Santagati, F. Stefanini, and M. Viale, Proc. Natl. Acad. Sci. U.S.A. **107**, 11865 (2010).
[2] W. Bialek, A. Cavagna, I. Giardina, T. Mora, E. Silvestri, M. Viale, and A. M. Walczak, Proc. Natl. Acad. Sci. U.S.A. **109**, 4786 (2012).
[3] A. Bricard, J.-B. Caussin, N. Desreumaux, O. Dauchot, and D. Bartolo, Nature (London) **503**, 95 (2013).
[4] C. A. Weber, T. Hanke, J. Deseigne, S. Léonard, O. Dauchot, E. Frey, and H. Chaté, Phys. Rev. Lett. **110**, 208001 (2013).
[5] E. Ferrante, A. E. Turgut, M. Dorigo, and C. Huepe, Phys. Rev. Lett. **111**, 268302 (2013).
[6] Y. Zheng, C. Huepe, and Z. Han, Adaptive Behavior **30**, 19 (2022).
[7] E. F. Teixeira, H. C. M. Fernandes, and L. G. Brunnet, Soft Matter **17**, 5991 (2021).
[8] G. Flierl, D. Grünbaum, S. Levins, and D. Olson, J. Theor. Biol. **196**, 397 (1999).
[9] S. Liu, S. Shankar, M. C. Marchetti, and Y. Wu, Nature (London) **590**, 80 (2021).
[10] A. Bricard, J.-B. Caussin, D. Das, C. Savoie, V. Chikkadi, K. Shitara, O. Chepizhko, F. Peruani, D. Saintillan, and D. Bartolo, Nat. Commun. **6**, 1 (2015).
[11] A. Chardac, L. A. Hoffmann, Y. Poupart, L. Giomi, and D. Bartolo, Phys. Rev. X **11**, 031069 (2021).
[12] J. Toner, Y. Tu, and S. Ramaswamy, Ann. Phys. (Amsterdam) **318**, 170 (2005).
[13] J. Toner, Phys. Rev. E **86**, 031918 (2012).
[14] S. Henkes, Y. Fily, and M. C. Marchetti, Phys. Rev. E **84**, 040301(R) (2011).
[15] N. Shimoyama, K. Sugawara, T. Mizuguchi, Y. Hayakawa, and M. Sano, Phys. Rev. Lett. **76**, 3870 (1996).
[16] G. Grégoire and H. Chaté, Phys. Rev. Lett. **92**, 025702 (2004).

[17] H. Xu, Y. Huang, R. Zhang, and Y. Wu, Nat. Phys. **19**, 46 (2023).
[18] B. Szabó, G. J. Szöllösi, B. Gönci, Z. Jurányi, D. Selmeczi, and T. Vicsek, Phys. Rev. E **74**, 061908 (2006).
[19] G. Peyret, R. Mueller, J. d'Alessandro, S. Begnaud, P. Marcq, R.-M. Mège, J. M. Yeomans, A. Doostmohammadi, and B. Ladoux, Biophys. J. **117**, 464 (2019).
[20] E. Ferrante, A. E. Turgut, M. Dorigo, and C. Huepe, Phys. Rev. Lett. **111**, 268302 (2013).
[21] F. G. Woodhouse, H. Ronellenfitsch, and J. Dunkel, Phys. Rev. Lett. **121**, 178001 (2018).
[22] P. Baconnier, D. Shohat, C. H. López, C. Coulais, V. Démery, G. Düring, and O. Dauchot, Nat. Phys. **18**, 1234 (2022).
[23] E. Zheng, M. Brandenbourger, L. Robinet, P. Schall, E. Lerner, and C. Coulais, Phys. Rev. Lett. **130**, 178202 (2023).
[24] X. Mao and T. C. Lubensky, Annu. Rev. Condens. Matter Phys. **9**, 413 (2018).
[25] M. Davidescu, P. Romanczuk, T. Gregor, and I. Couzin, Proc. Natl. Acad. Sci. U.S.A. **120**, e2206163120 (2023).
[26] R. D. Resch, Geometrical device having articulated relatively movable sections, United States of America Patent No. 3201894 (Aug. 24, 1965).
[27] J. N. Grima and K. E. Evans, J. Mater. Sci. Lett. **19**, 1563 (2000).
[28] D. Acuna, F. Gutiérrez, R. Silva, H. Palza, A. S. Nunez, and G. Düring, Commun. Phys. **5**, 1 (2022).
[29] M. Czajkowski, C. Coulais, M. van Hecke, and D. Rocklin, Nat. Commun. **13**, 1 (2022).
[30] See Supplemental Material at http://link.aps.org/supplemental/10.1103/PhysRevLett.132.238303 for mathematical derivations and movies.
[31] M. Brandenbourger, C. Scheibner, J. Veenstra, V. Vitelli, and C. Coulais, arXiv:2108.08837.
[32] O. Dauchot and V. Démery, Phys. Rev. Lett. **122**, 068002 (2019).
[33] A. Bossart, D. M. J. Dykstra, J. van der Laan, and C. Coulais, Proc. Natl. Acad. Sci. U.S.A. **118**, e2018610118 (2021).